Tunable multiwindow magnomechanically induced transparency, Fano resonances, and slow-to-fast light conversion — Source link

Kamran Ullah, M. Tahir Naseem, Özgür E. Müstecaplıoğlu

Institutions: Koç University

Related papers:

- Phase control of the transmission in cavity magnomechanical system with magnon driving

- High Cooperativity Cavity QED with Magnons at Microwave Frequencies

- Electromagnetically induced transparency in mechanical effects of light

- Magnetically controllable slow light based on magnetostrictive forces.

- Cavity Optomechanics

Tunable multiwindow magnomechanically induced transparency, Fano resonances, and slow-to-fast light conversion

Kamran Ullah [ORCID],[*] M. Tahir Naseem [ORCID],[†] and Özgür E. Müstecaplıoğlu [ORCID][‡]

Department of Physics, Koç University, Sarıyer, İstanbul 34450, Turkey

We investigate the absorption and transmission properties of a weak probe field under the influence of a strong control field in a cavity magnomechanical system. The system consists of two ferromagnetic-material yttrium iron garnet (YIG) spheres coupled to a single cavity mode. In addition to two magnon-induced transparencies (MITs) that arise due to magnon-photon interactions, we observe a magnomechanically induced transparency (MMIT) due to the presence of nonlinear magnon-phonon interaction. We discuss the emergence of Fano resonances and explain the splitting of a single Fano profile to double and triple Fano profiles due to additional couplings in the proposed system. Moreover, by considering a two-YIG system, the group delay of the probe field can be enhanced by one order of magnitude as compared with a single-YIG magnomechanical system. Furthermore, we show that the group delay depends on the tunability of the coupling strength of the first YIG with respect to the coupling frequency of of the second YIG, and vice versa. This helps to achieve larger group delays for weak magnon-photon coupling strengths.

I. INTRODUCTION

Storing information in different frequency modes of light has attracted much attention due to its critical role in high-speed, long-distance quantum communication applications [1–3]. The spectral distinction of optical signals eliminates their unintentional coupling to the stationary information or memory nodes in a communication network. For that aim, multiple-transparency-window electromagnetically induced transparency (EIT) schemes have been considered for multiband quantum memory implementations, mainly in the medium of three-level cold atoms. Experimental demonstrations of three EIT windows have been reported [4] and extended to seven windows by using external fields [5]. Observation of nine EIT windows has been experimentally demonstrated quite recently by using an external magnetic field in a vapor cell of Rubidium atoms [6]. A practical question is if such results can be achieved at higher temperatures, for example, for a room-temperature multiband quantum memory.

In recent years, remarkable developments have been achieved to strongly couple spin ensembles to cavity photons, leading to the emerging field of cavity spintronics. Quanta of spin waves (magnons) are highly robust against temperature [7–11], and hence significant magnon-photon hybridization and magnetically induced transparency (MIT) have been successfully demonstrated even at room temperature [11]. Tunable slow light and its conversion to fast light based on room-temperature MIT has been theoretically shown recently

[12]. Besides, at strong magnon-photon interaction, a wide tunability of slow light via an applied magnetic field has been shown in Ref. [13]. These results demonstrate the promising value of these systems for practical quantum memories [12]. Here we explore how to split such a MIT window into multiple bands for a room-temperature multimode quantum memory. Our idea is to exploit the coupling of magnons to thermal vibrations, which is known to yield magnomechanically induced transparency (MMIT) [14], in combination with multiple spin ensembles, to achieve multiple bands in MIT. We also discuss the emergence of the Fano resonance in the output spectrum and explore the suitable system parameters for its observation. The Fano resonance was first reported in atomic systems [15], and it emerges due to the quantum interference of different transition amplitudes which give minima in the absorption profile. In later years, it was discussed in different physical systems, such as photonic crystals [16], coupled microresonators [17], and optomechanical systems [18]. Recently, Fano-like asymmetric shapes have been experimentally reported in a hybrid cavity magnomechanical system [14].

Our model consists of two ferromagnetic insulators; specifically, yttrium iron garnets (YIGs), hosting long-lived magnons at room temperature, placed inside a three-dimensional (3D) microwave cavity; we remark that another equivalent embodiment of our model could be to place the YIGs on top of a superconducting coplanar waveguide, which can have further practical significance being an on-chip device [19]. Specific benefits of YIG as the host of spin ensembles over other systems, such as paramagnetic spin ensembles in nitrogen-vacancy centers, is due to its high spin density of 2.1×10^{22} μB/cm^3 (μB is the Bohr magneton) and high room-temperature spin polarization below the Curie temperature (559 K). In addition to multimode quantum memories,

*kamran@phys.qau.edu.pk
†mnaseem16@ku.edu.tr
‡omustecap@ku.edu.tr

our results can be directly advantageous for readily integrated microwave circuit applications at room temperature, such as multimode quantum transducers coupling different systems at different frequencies [20], tunable-frequency quantum sensors [21], or fast light enhanced gyroscopes [22]. In addition to the magnetic-dipole interaction between the cavity field and the spin ensemble, we take into account coupling between the magnons and the quanta of YIG lattice vibrations (phonons) arising due to the magnetostrictive force [14]. We only consider the Kittel mode [23] of the ferromagnetic resonance modes of the magnons. Such three-body quantum systems can be of fundamental significance to examine macroscopic quantum phenomena towards the thermodynamic limit and quantum-to-classical transitions [24].

In our model, tunable slow and fast light emerges as a natural consequence of tunable splitting of the MIT window. Slow-light propagation at room temperature has been investigated recently in a cavity-magnon system and the group delays are found to be in the μs range [12]. In a single YIG magnomechanical system with strong magnon-photon coupling strength, slow light was achieved with a maximum group delay of <0.8 ms [13]. In this paper, we discuss slow and fast light in a two-YIG magnomechanical system. Furthermore, we explain that the group delay depends on the tunability of the magnon-photon coupling of the first YIG (YIG1) with respect to the magnon-photon coupling of the second YIG (YIG2). This not only helps achieve larger group delays at weak magnon-photon coupling, but also increases the group delay of the transmitted probe field by one order of magnitude, which is not possible with a single-YIG system [13].

The rest of the paper is organized as follows: We describe the model system in Sec. II and present dynamical equations with steady-state solutions. The results and discussions for MMIT are presented in the Sec. III. We discuss the emergence and tunability of the multiple Fano resonances in Sec. IV. Next, in Sec. V, we present the transmission of the probe field and discuss the group delays for slow and fast light propagation. Finally, in Sec. VI, we present the conclusion of our work.

II. SYSTEM HAMILTONIAN AND THEORY

We consider a hybrid cavity magnomechanical system that consists of two YIG spheres placed inside a microwave cavity, as shown in Fig. 1. A uniform bias magnetic field (z direction) is applied on each sphere, which excites the magnon modes, and these modes are coupled with the cavity field via magnetic-dipole interactions. The excitation of the magnon modes inside the spheres leads to a variable magnetization that results in the deformation of their lattice structure. The magnetostrictive force causes vibrations of the YIGs, which establishes magnon-phonon interactions in these spheres. The single-magnon magnomechanical coupling strength is very weak [14] and depends on the sphere diameter and the direction of the external bias field. Either by considering a larger YIG1 sphere or by adjusting the direction of the bias magnetic field on it, the magnomechanical coupling of this sphere can be ignored [24]. Here, we assume that the direction of the bias field on YIG1 is such that the single-magnon magnome-
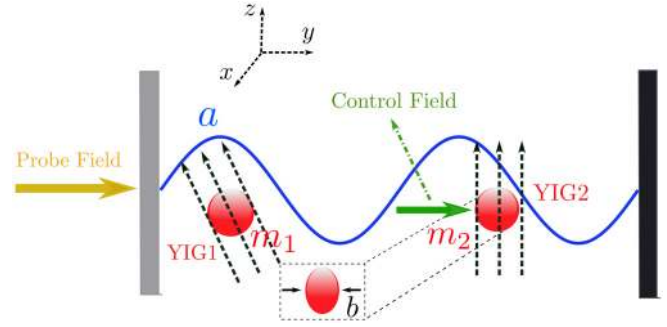

FIG. 1. A schematic illustration of a hybrid cavity magnomechanical system. It consists of two ferromagnetic yttrium iron garnet (YIG) spheres placed inside a microwave cavity. A bias magnetic field is applied in the z direction on each sphere, which excites the magnon modes, and these modes are strongly coupled with the cavity field. The bias magnetic field activates the magnetostrictive (magnon-phonon) interaction in both YIGs. The single-magnon magnomechanical coupling strength is very weak [14], and it depends on the sphere diameters and the external bias field direction. Either by considering a larger YIG1 sphere or by adjusting the direction of the bias field on it, the magnomechanical coupling of this sphere can be ignored. Here, we assume that the direction of the bias field at YIG1 is such that the single-magnon magnomechanical interaction becomes very weak and can be ignored [14]. However, the magnomechanical interaction of YIG2 is enhanced by directly driving its magnon mode via a microwave drive (y direction). This microwave drive plays the role of a control field in our model. Cavity, phonon, and magnon modes are labeled a, b, and m_i ($i = 1, 2$), respectively.

chanical interaction becomes very weak and can be ignored [14]. However, the magnomechanical interaction of YIG2 is enhanced by directly driving its magnon mode via an external microwave drive. This microwave drive plays the role of a control field in our model. In addition, the cavity is driven by a weak probe field.

In this work, we consider high-quality YIG spheres, each 250 μm in diameter and composed of ferric ions Fe^{+3} of density $\rho = 4.22 \times 10^{27}$ m^{-3}. This causes a total spin $S = 5/2\rho V_m = 7.07 \times 10^{14}$, where V_m is the volume of the YIG and S is the collective spin operator which satisfies the algebra $[S_\alpha, S_\beta] = i\varepsilon^{\alpha\beta\gamma}S_\gamma$. The Hamiltonian of the system reads [24]

$$
\begin{aligned}
H/\hbar = \ & \omega_a \hat{a}^\dagger \hat{a} + \omega_b \hat{b}^\dagger \hat{b} + \sum_{j=1}^{2}[\omega_j \hat{m}_j^\dagger \hat{m}_j + g_j(\hat{m}_j^\dagger \hat{a} + m_j \hat{a}^\dagger)] \\
& + g_{mb}\hat{m}_2^\dagger \hat{m}_2(\hat{b} + \hat{b}^\dagger) + i(\Omega_d \hat{m}_2^\dagger e^{-i\omega_d t} - \Omega_d^\star \hat{m}_2 e^{i\omega_d t}) \\
& + i(\hat{a}^\dagger \varepsilon_p e^{-i\omega_p t} - \hat{a}\varepsilon_p^\star e^{i\omega_p t}),
\end{aligned}
\tag{1}
$$

where $a^\dagger$ (a) and $b^\dagger$ (b) are the creation (annihilation) operators of the cavity and phonon modes, respectively. The resonance frequencies of the cavity, phonon, and magnon modes are denoted ω_a, ω_b, and ω_j, respectively. Moreover, m_j is the bosonic operator of the Kittle mode of frequency ω_j and its coupling strength with the cavity mode is given by g_j. The frequency ω_j of the magnon mode m_j can be determined by using the gyromagnetic ratio γ_j and an external bias magnetic field H_j, i.e., $\omega_j = \gamma_j H_j$ with $\gamma_j/2\pi = 28$ GHz. The Rabi

frequency $\Omega_d = \sqrt{5}/4\gamma\sqrt{N}B_0$ [23] represents the coupling strength of the drive field of amplitude B_0 and frequency ω_d. Furthermore, in Eq. (1), ω_p is the probe field frequency with amplitude ε_p which can be expressed as $\varepsilon_p = \sqrt{2P_p\kappa_a/\hbar\omega_p}$.

Note that, in Eq. (1), we have ignored the nonlinear term $K\hat{m}_j^\dagger\hat{m}_j^\dagger\hat{m}_j\hat{m}_j$ that may arise due to a strongly driven magnon mode [25,26]. To ignore this nonlinear term, we must have $K|\langle m_2\rangle|^3 \ll \Omega$, and for the system parameters we consider in this work, this condition is always satisfied. The Hamiltonian in Eq. (1) is written after applying the rotating-wave approximation, in which fast oscillating terms $g_j(\hat{a}\hat{m}_j + \hat{a}^\dagger\hat{m}^\dagger)$ are dropped. This is valid for $\omega_a, \omega_j \gg g_j, \kappa_a, \kappa_{mj}$ which is the case to be considered in the present work (κ_a and κ_{mj} are the decay rates of the cavity and magnon modes, respectively). In the frame rotating at the drive frequency ω_d, the Hamiltonian of the system is given by

$$H/\hbar = \Delta_a\hat{a}^\dagger\hat{a} + \omega_b\hat{b}^\dagger\hat{b} + \sum_{j=1}^{2}[\Delta_{mj}\hat{m}_j^\dagger\hat{m}_j + g_j(\hat{m}_j^\dagger\hat{a} + m_j\hat{a}^\dagger)]$$
$$+ g_{mb}\hat{m}_2^\dagger\hat{m}_2(\hat{b} + \hat{b}^\dagger) + i(\Omega_d\hat{m}_2^\dagger - \Omega_d^\star\hat{m}_2)$$
$$+ i(\hat{a}^\dagger\varepsilon_p e^{-i\delta t} - \hat{a}\varepsilon_p^\star e^{i\delta t}), \qquad (2)$$

where $\Delta_a = \omega_a - \omega_d$, $\Delta_{mj} = \omega_j - \omega_d$, and $\delta = \omega_p - \omega_d$. The quantum Heisenberg-Langevin equations based on the Hamiltonian (2) can be written as

$$\dot{\hat{a}} = -i\Delta_a\hat{a} - i\sum_{j=1}^{2}g_j\hat{m}_j - \kappa_a\hat{a} + \varepsilon_p e^{-i\delta t} + \sqrt{2\kappa_a}\hat{a}^{\text{in}}(t),$$

$$\dot{\hat{b}} = -i\omega_b\hat{b} - ig_{mb}\hat{m}_2^\dagger\hat{m}_2 - \kappa_b\hat{b} + \sqrt{2\kappa_b}\hat{b}^{\text{in}}(t),$$

$$\dot{\hat{m}}_1 = -i\Delta_{m1}\hat{m}_1 - ig_1\hat{a} - \kappa_{m1}m_1 + \sqrt{2\kappa_{m1}}\hat{m}_1^{\text{in}}(t),$$

$$\dot{\hat{m}}_2 = -i\Delta_{m2}\hat{m}_2 - ig_2\hat{a} - \kappa_{m2}m_2 - ig_{mb}\hat{m}_2(\hat{b} + \hat{b}^\dagger)$$
$$+ \Omega_d + \sqrt{2\kappa_{m2}}\hat{m}_2^{\text{in}}(t), \qquad (3)$$

where κ_b is the dissipation rate of the phonon mode, and $\hat{b}^{\text{in}}(t)$, $\hat{m}_j^{\text{in}}(t)$, and $\hat{a}^{\text{in}}(t)$ are the vacuum input noise operators, which have zero mean values, i.e., $\langle\hat{q}_{\text{in}}\rangle = 0$ ($q = a, m, b$) [27,28]. The magnon mode m_2 is strongly driven by a microwave drive that causes a large steady-state amplitude $|\langle m_{2s}\rangle| \gg 1$ of the magnon mode, and due to the beam splitter interaction, this leads to a large steady-state amplitude of the cavity mode $|\langle a_s\rangle| \gg 1$. Consequently, we can linearize the quantum Langevin equations around the steady-state values and take only the first-order terms in the fluctuating operator: $\langle\hat{O}\rangle = O_s + \hat{O}_- e^{-i\delta t} + \hat{O}_+ e^{i\delta t}$ [29], where $\hat{O} = a, b, m_j$. First, we consider the zero-order solution, namely, steady-state solutions, which are given by

$$a_s = -i\sum_{1,2}\frac{g_j m_{js}}{\kappa_a + i\Delta_a},$$

$$b_s = \frac{-ig_{mb}|m_2 s|^2}{\kappa_b + i\omega_b},$$

$$m_{1s} = \frac{-ig_1 a_s}{\kappa_{m1} + i\Delta_{m1}}, \quad m_{2s} = \frac{\Omega_d - ig_2 a_s}{\kappa_{m2} + i\tilde{\Delta}_{m2}},$$

$$\tilde{\Delta}_{m2} = \Delta_{m2} + g_{mb}(b_s + b_s^\star). \qquad (4)$$

We assume that the coupling of the external microwave drive on magnon mode m_2 is much stronger than the amplitude ϵ_p of the probe field. Under this assumption, the linearized quantum Langevin equations can be solved by considering the first-order perturbed solutions and ignoring all higher-order terms of ϵ_p. The solution for the cavity mode is given by

$$a_- = \varepsilon_p\left[A' + C_1' + \frac{g_2^2}{\beta'} + \frac{\alpha^\star\alpha'}{\beta^\star\beta' + A^\star - C_1^\star + \frac{g_2^2}{\beta^\star}}\right]^{-1}, \quad (5)$$

where

$$A = \kappa_a + i(\Delta_a + \delta), \quad B = \frac{G_{mb}^2\omega_b}{\omega_b^2 - \delta^2 + i\delta\kappa_b},$$

$$C_1 = \frac{g_1^2}{\kappa_{m1} + i(\Delta_{m1} + \delta)}, \quad C_2 = \frac{g_2^2}{\kappa_{m2} + i(\tilde{\Delta}_{m2} + \delta)},$$

$$A' = \kappa_a + i(\Delta_a - \delta), \quad B' = \frac{G_{mb}^2\omega_b}{\omega_b^2 - \delta^2 - i\delta\kappa_b},$$

$$C_1' = \frac{g_1^2}{\kappa_{m1} + i(\Delta_{m1} - \delta)}, \quad C_2' = \frac{g_2^2}{\kappa_{m2} + i(\tilde{\Delta}_{m2} - \delta)},$$

$$\alpha = \frac{g_2^2 B}{C_2 + iB}, \quad \alpha' = \frac{g_2^2 B'}{C_2' + iB'},$$

$$\beta = C_2 - i\frac{C_2^\star B}{C_2^\star + iB}, \quad \beta' = C_2' - i\frac{C_2^\star B'}{C_2^\star + iB'}.$$

Here $G_{mb} = i\sqrt{2}g_{mb}m_{2s}$ is the effective magnon-phonon coupling. We use the input-output relation for the cavity field $\varepsilon_{\text{out}} = \varepsilon_{\text{in}} - 2\kappa_a\langle a\rangle$ [30], and the amplitude of the output field can be written as

$$\varepsilon_{\text{out}} = \frac{2\kappa_a a_-}{\varepsilon_p}. \qquad (6)$$

The real and imaginary parts of ε_{out} account for in-phase (absorption) and out-of-phase (dispersion) output field quadratures at the probe frequency.

III. MAGNOMECHANICALLY INDUCED TRANSPARENCY WINDOW PROFILES

For the numerical calculation, we use parameters from a recent experiment on a hybrid magnomechanical system [14], unless stated differently. The frequency of the cavity field $\omega_a/2\pi = 10$ GHz, $\omega_b/2\pi = 10$ MHz, $\kappa_b/2\pi = 100$ Hz, $\omega_{1,2}/2\pi = 10$ GHz, $\kappa_a/2\pi = 2.1$ MHz, $\kappa_{m1}/2\pi = \kappa_{m2}/2\pi = 0.1$ MHz, $g_1/2\pi = g_2/2\pi = 1.5$ MHz, $G_{mb}/2\pi = 3.5$ MHz, $\Delta_a = \omega_b$, $\Delta_{mj} = \omega_b$, and $\omega_d/2\pi = 10$ GHz.

We first illustrate the physics behind the multiband transparency by systematically investigating the role of different couplings in the model. Figure 2 displays the response of the probe field in the absorption spectrum of the output field for different coupling strengths. In Fig. 2(a), we assume that the magnon-phonon coupling (g_{mb}) and magnon mode m_1 coupling (g_1) with the cavity are absent. Therefore, only magnon mode m_2 is coupled with the cavity. Under these considerations, we observe a MIT in which a typical Lorentzian peak of the output spectrum of the simple cavity splits into two peaks with a single dip, as shown in Fig. 2(a). The width of
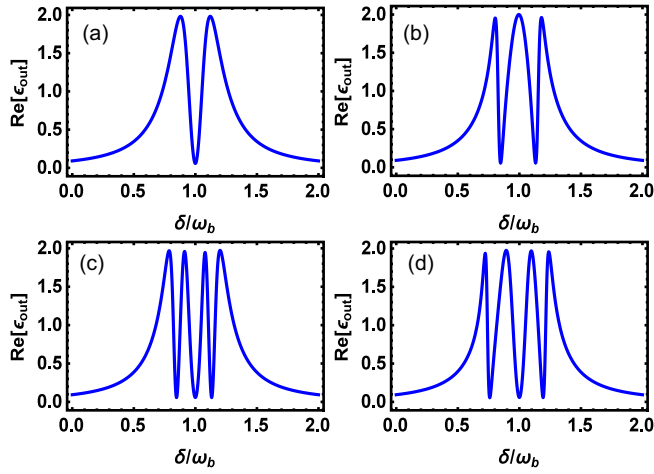
FIG. 2. Absorption Re[ε_{out}] profiles are shown against the normalized probe field detuning δ/ω_b. (a) $g_1 = g_{mb} = 0$, $g_2/2\pi = 1.2$ MHz and (b) $g_1 = 0$, $g_2/2\pi = 1.2$ MHz, $G_{mb}/2\pi = 2.0$ MHz, (c) $g_1/2\pi = g_2/2\pi = 1.2$ MHz, $G_{mb}/2\pi = 2$ MHz and (d) $g_1/2\pi = g_2/2\pi = 1.2$ MHz, $G_{mb}/2\pi = 3.5$ MHz. The other parameters are given in Sec. III.

FIG. 3. Dispersion Im[ε_{out}] profiles are shown versus the normalized probe field detuning δ/ω_b. (a) $g_1 = g_{mb} = 0$ and $g_2/2\pi = 1.2$ MHz and (b) $g_1 = 0$, $g_2/2\pi = 1.2$ MHz, $G_{mb}/2\pi = 2.0$ MHz (c), (d) $g_1/2\pi = g_2/2\pi = 1.2$ MHz, and (c) $G_{mb}/2\pi = 2$ MHz and (d) $G_{mb}/2\pi = 3.5$ MHz. The other parameters are given in Sec. III.

this transparency window can be controlled by tuning the microwave driving field power and the magnon-photon coupling g_2. Upon increasing the coupling strength g_2 the width of the window increases, and vice versa.

We observe two transparency windows in the absorption as we switch on the magnon-phonon coupling (g_{mb}) and keep $g_1 = 0$. Due to the nonzero magnetostrictive interaction, the single MIT window in Fig. 2(a) splits into the double window shown in Fig. 2(c). The right transparency window in Fig. 2(c) is associated with the magnon-phonon interaction, and this is the so-called magnomechanically induced transparency (MMIT) [14] window. We can observe the double MIT by removing the magnon-phonon coupling g_{mb}, and considering nonzero couplings between the magnon modes and the cavity field.

Finally, if we consider all three couplings simultaneously to be nonzero, then the transparency window splits into three windows consisting of four peaks and three dips; this is shown in Fig. 2(c). In this case, one window is associated with the magnomechanical interaction, and the other two are induced by magnon-photon couplings. The width and peak separations of these windows increases and broadens, respectively, at higher values of magnon-phonon coupling G_{mb}, which can be seen in Fig. 2(d). Moreover, we have a symmetric multiwindow transparency profile where the splitting of the peaks occurs at side-mode frequencies $\omega_p = \omega_b \pm \omega_d$.

In Figs. 3(a)–3(d), we plot the dispersion spectrum of the output field versus the normalized frequency of the probe field. The single MIT dispersion spectrum in the absence of YIG1 and the magnon-phonon coupling g_{mb} is shown in Fig. 3(a). The dispersion spectra for the case of $g_1 = 0$, $g_2 \neq 0$, and $g_{mb} \neq 0$ is plotted in Fig. 3(b). In the presence of all three couplings, the dispersion spectrum of the output field is given in Figs. 3(c) and 3(d). It is clear from Figs. 3(c) and 3(d), by the increase in the effective magnon-phonon coupling G_{mb}, that the transparency windows become wider. We point out
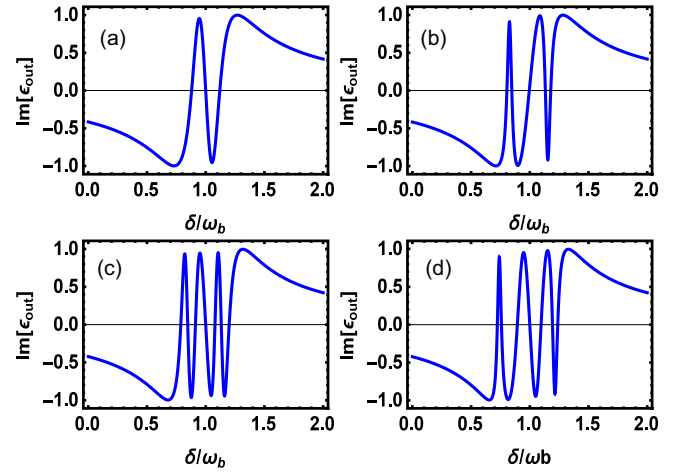
that the magnomechanically induced amplification (MMIA) of the output field in our system can be obtained in the blue-detuned regime; $\Delta_{m2} = -\omega_b$.

IV. FANO RESONANCES IN THE OUTPUT FIELD

In the following, we discuss the emergence and physical mechanism of the Fano lineshapes in the output spectrum. The shape of the Fano resonance is distinctly different from the symmetric resonance curves in the EIT, MIT, optomechanically induced transparency (OMIT), and MMIT windows [14,31]. The Fano resonance has been observed in systems in which EIT was reported by a suitable selection of the system parameters [14,31–36]. The physical origin of the Fano resonance in systems having optomechanical-like interactions has been explained as due to the presence of nonresonant interactions. For example, in a standard optomechanical system, if the anti-Stokes process is not resonant with the cavity frequency, asymmetric Fano shapes appear in the spectrum [31–33]. In our system, this corresponds to $\Delta_{m1} \neq \omega_b$ because, instead of a cavity mode, the magnon mode m_1 is coupled with a phonon mode via an optomechanical-like interaction. The asymmetric Fano shapes can be seen in Figs. 4(a)–4(c) for different nonresonant cases, where the absorption spectrum of the output field as a function of normalized detuning δ/ω_b is shown. In Fig. 4(a), we consider $g_1 = g_{mb} = 0$, and coupling of the magnon mode m_2 with the cavity is nonzero. Due to the presence of a nonresonant process ($\Delta_{m2} = 0.7\omega_m$), the absorption spectrum of the symmetric MIT profile [Fig. 2(a)] changes into an asymmetric-window profile, as shown in Fig. 4(a). Such an asymmetric MIT band can be related to a Fano-like resonance, emerging frequently in optomechanical systems [31–35]. If we remove YIG1 and consider only that YIG2 is coupled with the cavity mode and $\Delta_{m2} = 0.7\omega_m$, then we observe a double Fano resonance in the output spectrum, which is shown in Fig. 4(b). Similarly, in the presence of all three couplings
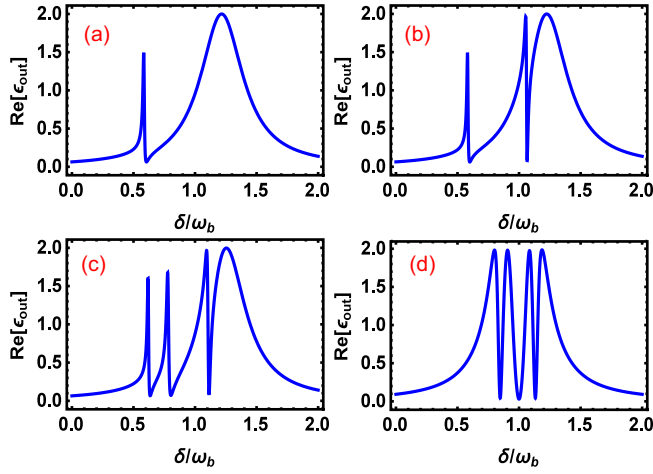
FIG. 4. Fano lineshapes in the asymmetric absorption $\text{Re}[\varepsilon_{out}]$ profiles are shown versus the normalized probe frequency δ/ω_b. (a) $\Delta_{m2} = 0.7\omega_b$, $g_2 = 1.5$ MHz, $g_1 = g_{mb} = 0$, and (b) $\Delta_{m2} = 0.7\omega_b$, $g_1 = 0$, $g_2 = 1.5$ MHz, $G_{mb} = 3.5$ MHz. (c) $\Delta_{m1,2} = 0.7\omega_b$, $g_1 = g_2/2\pi = 1.5$ MHz and $G_{mb}/2\pi = 3.5$ MHz, and (d) $\Delta_{m1,2} = \omega_b$, $g_1 = g_2/2\pi = 1.5$ MHz and $G_{mb}/2\pi = 3.5$ MHz. In all panels, $g_1 = g_2/2\pi = 1.5$ MHz, $G_{mb}/2\pi = 3.5$ MHz, and rest of the parameters are given in Sec. III.

and with $\Delta_{m1,m2} = 0.7\omega_m$, the double Fano resonance goes over to a triple Fano resonance, as shown in Fig. 4(c). This is because the cavity field can be built up by three coherent routes provided by the three coupled systems (the magnons, cavity, and phonon modes), and they can interfere with each other. The Fano resonances disappear when we consider a resonant case $\Delta_{m1} = \Delta_{m2} = \omega_b$, as shown in Fig. 4(d).

V. NUMERICAL RESULTS FOR SLOW AND FAST LIGHT

Here we investigate the transmission and group delay of the output signal and show the effect of the magnon-photon and magnon-phonon couplings on the transmission spectrum. From Eq. (6), the rescaled transmission field corresponding to the probe field can be expressed as

$$t_p = \frac{\varepsilon_p - 2\kappa_a a_-}{\varepsilon_p}. \tag{7}$$

In Figs. 5(a)–5(d), we plot the transmission spectrum of the probe field against the scaled detuning δ/ω_b, for different values of g_1. It is clear from Fig. 5(a), that the transmission peak associated with the magnon-photon coupling of YIG1 is smaller than the two other peaks. This is because, in Fig. 5(a), g_1 coupling is weaker than the other two interactions g_2 and G_{mb} present in the system. By increasing the coupling strength g_1, the peak of the middle transparency profile grows in height and reaches close to unity, as shown in Figs. 5(b) and 5(c). In addition, Fig. 5(d) shows that the width of the transparency window can be increased at higher higher values of the magnon-photon coupling g_1. In Figs. 6(a) and 6(b), the transmission spectrum of the probe field as a function of dimensionless detuning is shown for different values of G_{mb}. In Figs. 6(a) and 6(b), we consider both g_1 and g_2 to be the same in the strong-coupling regime. However, the effective
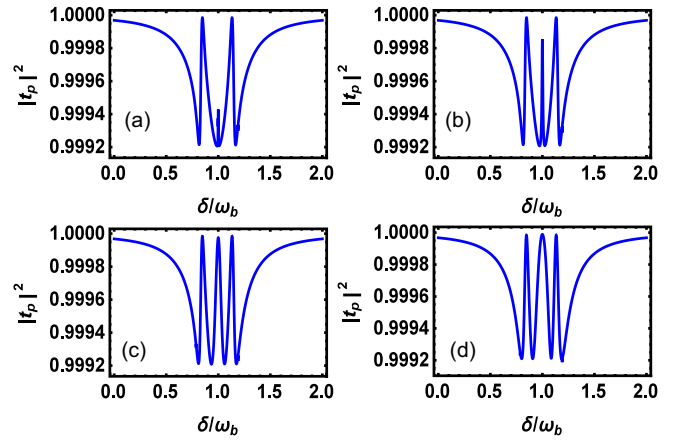

FIG. 5. The transmission $|t_p|^2$ spectrum as a function of normalized probe field frequency δ/ω_b is shown for different values of g_1. (a) $g_1/2\pi = 0.5$ MHz, (b) $g_1/2\pi = 0.8$ MHz, (c) $g_1/2\pi = 1.2$ MHz, (d) $g_1/2\pi = 1.5$ MHz. In all panels, $g_2/2\pi = 1.5$ MHz, $G_{mb}/2\pi = 3.5$ MHz, and the other parameters are given in Sec. III.

coupling $\tilde{g}_2 = g_2\alpha_s$ depends on the steady-state amplitude of the cavity field α_s, which depends on the m_{2s}. Consequently, $\tilde{g}_2$ and G_{mb} are related, as can be seen from Eq. (4). For a smaller value of G_{mb} in Fig. 6(a), we have two small peaks associated with g_2 and G_{mb}; in addition, the third-highest peak is associated with g_1. For a fixed value of g_{mb}, if we increase G_{mb}, it increases $\tilde{g}_1$, and the peaks associated with these two couplings become more visible, as shown in Fig. 6(b). Similarly, in Figs. 6(c) and 6(d), we observe a similar increase in the height of two peaks associated with g_2 and G_{mb}, for the variation in g_2.

The phase ϕ_t of the transmitted probe field t_p is given by the relation $\phi_t = \text{Arg}[t_p]$. The plot of ϕ_t as a function of normalized detuning δ/ω_b is shown in Fig. 7. In the inset of Fig. 7(a), we consider that both g_1 and g_{mb} are switched off, and only g_2 is nonzero. This gives a conventional phase of the transmitted field with a single MIT curve, which appears
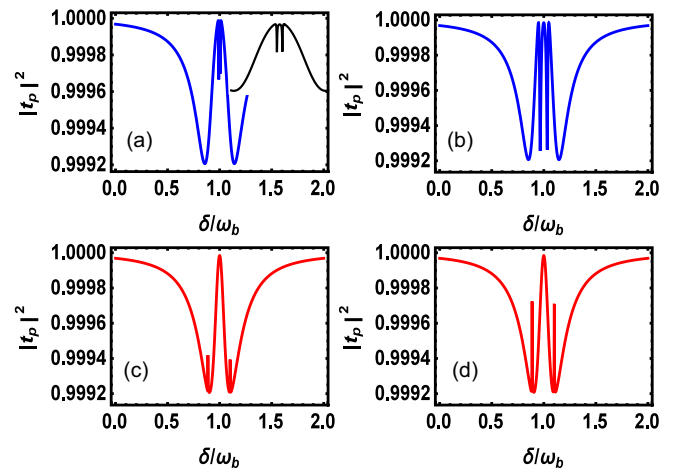

FIG. 6. . The transmission $|t_p|^2$ spectrum as a function of the normalized probe field frequency δ/ω_b. (a) $G_{mb}/2\pi = 0.5$ MHz, (b) $G_{mb}/2\pi = 1.0$ MHz. (c) $g_2/2\pi = 0.4$ MHz, (d) $g_2/2\pi = 0.8$ MHz. The other parameters are the same as in Fig. 5.
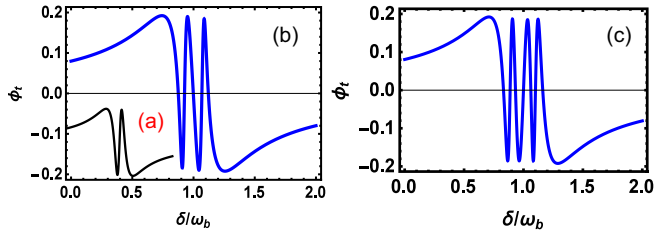
FIG. 7. The phase ϕ_t of the transmitted probe field versus normalized detuning δ/ω_b for different coupling strengths. (a) $g_1 = g_{mb} = 0$, (b) $g_1 = 0$, $g_2/2\pi = 1.5$ MHz, $G_{mb}/2\pi = 4$ MHz, (c) $g_1/2\pi = g_2/2\pi = 1.5$ MHz, and $G_{mb}/2\pi = 4$ MHz. The rest of parameters are given in Sec. III.

similar to the standard single OMIT curve [31]. In Fig. 7(b), we switch off the YIG1 coupling with the field ($g_1 = 0$), and the other two couplings are present ($g_{mb} \neq 0$, $g_2 \neq 0$), due to which the single transparency window splits into a double window. If we keep all three couplings nonzero, we get a triple transparency window, which is shown in Fig. 7(c).

The transmitted probe field phase is associated with the group delay τ_g of the output field and is defined as

$$\tau_g = \frac{\partial \phi(\omega_p)}{\partial \omega_p}, \qquad (8)$$

which means that a more rapid phase dispersion leads to larger group delays and vice versa. In addition, a negative slope of the phase represents a negative group delay or fast light ($\tau_g < 0$), whereas a positive slope of the transmitted field indicates positive group delay or slow light ($\tau_g > 0$). From Fig. 7, we observe that, in the regime of the narrow transparency window, there is a rapid variation in the probe phase, and this rapid phase dispersion can lead to a significant group delay.

Figure 8 shows that the group delay τ_g can be tuned by the variation of the bias magnetic field B_0 applied on YIG2. In the absence of YIG1 [Fig. 8(a)], we have a lower slope of Eq. (8); as a result, a maximum group delay of $\tau_g = 1$ ms is achieved. This group delay can be enhanced by one order of magnitude once the second YIG is introduced; see Fig. 8(b). The slope in Fig. 8(b) becomes steeper and the time delay for slow light is increased up to 13.8 ms. This shows that the two-YIG system is a good choice to observe a longer group delay in a magnomechanical system, while a single-YIG system cannot
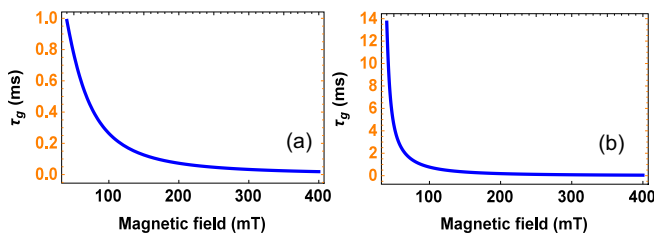

FIG. 8. Group delay τ_g of the output probe field plotted against the amplitude of the magnetic field B_0 for (a) $g_1 = 0$ and (b) $g_1/2\pi = 1.5$ MHz. The other parameter are $g_2/2\pi = 1.5$, $G_{mb}/2\pi = 3.5$ MHz, $\kappa_b/2\pi = 100$ Hz, $\kappa_{m1}/2\pi = \kappa_{m2}/2\pi = 0.1$ MHz, $\kappa_a/2\pi = 2.1$ MHz, and $\Omega_d = 1.2$ THz.
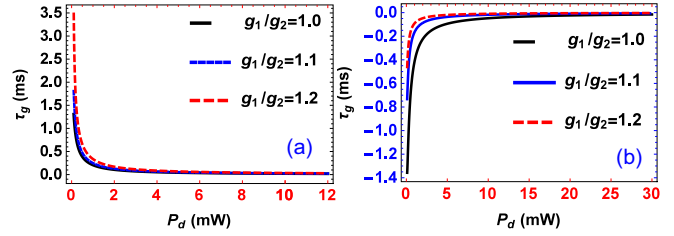

FIG. 9. The group delay τ_g of the transmitted probe field as a function of the driving power P_d for several values of magnon-photon coupling. (a) $\Delta_{m1} = \omega_b$, (b) $\Delta_{m1} = -\omega_b$, and the other parameter are the same as given in Fig. 8.

do so. Moreover, the numerical value of the group delay τ_g can be tuned from positive (slow light) to negative (fast light) by tuning the magnon-field detuning $\Delta_{m1} = \omega_b$ to $\Delta_{m1} = -\omega_b$. Here, it is worth mentioning that Fig. 8(b) can be switched into fast light with a maximum group delay on the order of $\tau_g \approx -1.4$ ms in the presence of both YIGs, but we do not show this in the figure. This negative group delay for the fast light propagation is one order of magnitude greater than a single-YIG magnomechanical system [13].

Finally, we investigate the control of group delay with the external microwave driving power and magnon-photon couplings. For this purpose, in Figs. 9(a) and 9(b), we plot τ_g against the driving power for different strengths of the magnon-photon coupling of YIG1 with respect to the coupling frequency of YIG2. Figure 9(a) shows that the magnitude of the group delay increases with the increase of g_1 corresponding to g_2, which indicates an enhanced group delay of the transmitted probe field in a two-YIG system. We tuned the coupling strenght of YIG1 (g_1) for different values by keeping the coupling strength of YIG2 (g_2) constant. This shows that increasing the magnon-photon coupling strength increases the group delay of the transmitted probe field and vice versa. This helps us to obtain larger group delays at relatively weak magnon-photon coupling strengths, which is not otherwise possible with a single-YIG magnomechanical system [13]. Similar results can also be obtained by increasing the magnon-photon coupling g_2 and fixing g_1. For the blue-detuned regime $\Delta_{m1} = -\omega_b$, group delay becomes negative. However, the effect of magnon-photon coupling remains the same, as shown in Fig. 9(b). From Figs. 8 and 9, we see that a two-YIG magnomechanical system provides not only extra tunability, but also drastically enhances the group delay compared with the single-YIG system studied in Ref. [13]. Our system can be used as a tunable switch, which can be controlled via different system parameters, and our results are comparable with the existing proposals based on various hybrid quantum systems [37–40].

VI. CONCLUSION

We have investigated the transmission and absorption spectrum of a weak probe field under a strong control field in a hybrid magnomechanical system in the microwave regime. Due to the presence of a nonlinear phonon-magnon interaction, we observed magnomechanically induced transparency (MMIT), and the photon-magnon interactions lead

to magnon-induced transparency (MIT). We found single MMIT, a result of the single-phonon process, and found two MIT windows in the output probe spectra due to the presence of two magnon-photon interactions. This is demonstrated by plotting the absorption, dispersion, and transmission of the output field. We discussed the emergence of Fano resonances in the output field spectrum of the probe field. These asymmetric lineshapes appeared due to the presence of anti-Stokes processes in the system. We examined conditions of slow and fast light propagation in our system, which can be controlled by different system parameters. It was shown that, in a two-YIG magnomechanical system, the tunability of the first coupling strength (YIG1) corresponding to the coupling of the second YIG (YIG2) has an immense effect on the slow and fast light and vice versa. This not only helped to investigate larger group delays at a weak magnon-photon coupling but also enhanced the group delay of the transmitted probe field, which is not possible in a single-YIG system. Our results suggest that this system may find applications to implement multiband quantum memories [12].

[1] M. Afzelius, C. Simon, H. de Riedmatten, and N. Gisin, Phys. Rev. A **79**, 052329 (2009).

[2] N. Sinclair, E. Saglamyurek, H. Mallahzadeh, J. A. Slater, M. George, R. Ricken, M. P. Hedges, D. Oblak, C. Simon, W. Sohler *et al.*, Phys. Rev. Lett. **113**, 053603 (2014).

[3] P. Jobez, N. Timoney, C. Laplane, J. Etesse, A. Ferrier, P. Goldner, N. Gisin, and M. Afzelius, Phys. Rev. A **93**, 032327 (2016).

[4] D. McGloin, M. H. Dunn, and D. J. Fulton, Phys. Rev. A **62**, 053802 (2000).

[5] K. Ying, Y. Niu, D. Chen, H. Cai, R. Qu, and S. Gong, J. Mod. Opt. **61**, 631 (2014).

[6] S. Bhushan, V. S. Chauhan, D. M, and R. K. Easwaran, Phys. Lett. A **383**, 125885 (2019).

[7] D. Zhang, X.-M. Wang, T.-F. Li, X.-Q. Luo, W. Wu, F. Nori, and J. You, npj Quantum Inf. **1**, 15014 (2015).

[8] Y. Tabuchi, S. Ishino, T. Ishikawa, R. Yamazaki, K. Usami, and Y. Nakamura, Phys. Rev. Lett. **113**, 083603 (2014).

[9] M. Goryachev, W. G. Farr, D. L. Creedon, Y. Fan, M. Kostylev, and M. E. Tobar, Phys. Rev. Applied **2**, 054002 (2014).

[10] H. Huebl, C. W. Zollitsch, J. Lotze, F. Hocke, M. Greifenstein, A. Marx, R. Gross, and S. T. B. Goennenwein, Phys. Rev. Lett. **111**, 127003 (2013).

[11] X. Zhang, C.-L. Zou, L. Jiang, and H. X. Tang, Phys. Rev. Lett. **113**, 156401 (2014).

[12] Z. Liu, H. Xiong, and Y. Wu, IEEE Access **7**, 57047 (2019).

[13] C. Kong, B. Wang, Z.-X. Liu, H. Xiong, and Y. Wu, Opt. Express **27**, 5544 (2019).

[14] X. Zhang, C.-L. Zou, L. Jiang, and H. X. Tang, Sci. Adv. **2**, e1501286 (2016).

[15] U. Fano, Phys. Rev. **124**, 1866 (1961).

[16] M. V. Rybin, A. B. Khanikaev, M. Inoue, K. B. Samusev, M. J. Steel, G. Yushin, and M. F. Limonov, Phys. Rev. Lett. **103**, 023901 (2009).

[17] Y.-F. Xiao, M. Li, Y.-C. Liu, Y. Li, X. Sun, and Q. Gong, Phys. Rev. A **82**, 065804 (2010).

[18] S. Kaur, B. Yao, Y.-S. Gui, and C.-M. Hu, J. Phys. D: Appl. Phys. **49**, 475103 (2016).

[19] R. Hisatomi, A. Osada, Y. Tabuchi, T. Ishikawa, A. Noguchi, R. Yamazaki, K. Usami, and Y. Nakamura, Phys. Rev. B **93**, 174427 (2016).

[20] N.-H. Kim, J. Jung, J. Cho, D.-S. Han, Y. Yin, J.-S. Kim, H. J. M. Swagten, and C.-Y. You, Appl. Phys. Lett. **108**, 142406 (2016).

[21] M. Huang, Y. Zhang, F. Li, L. Zhang, R. S. Ruoff, Z. Wen, and Q. Liu, Sci. Rep. **4**, 3878 (2014).

[22] C. Kittel, Phys. Rev. **73**, 155 (1948).

[23] J. Li, S.-Y. Zhu, and G. S. Agarwal, Phys. Rev. Lett. **121**, 203601 (2018).

[24] J. Li and S.-Y. Zhu, New J. Phys. **21**, 085001 (2019).

[25] Y.-P. Wang, G.-Q. Zhang, D. Zhang, T.-F. Li, C.-M. Hu, and J. Q. You, Phys. Rev. Lett. **120**, 057202 (2018).

[26] Y.-P. Wang, G.-Q. Zhang, D. Zhang, X.-Q. Luo, W. Xiong, S.-P. Wang, T.-F. Li, C.-M. Hu, and J. Q. You, Phys. Rev. B **94**, 224410 (2016).

[27] H. Xiong and Y. Wu, Appl. Phys. Rev. **5**, 031305 (2018).

[28] M. Aspelmeyer, T. J. Kippenberg, and F. Marquardt, Rev. Mod. Phys. **86**, 1391 (2014).

[29] S. Huang and G. S. Agarwal, Phys. Rev. A **83**, 043826 (2011).

[30] C. Gardiner and P. Zoller, *Quantum Noise: A Handbook of Markovian and Non-Markovian Quantum Stochastic Methods with Applications to Quantum Optics* (Springer Science & Business Media, Berlin, New York, 2004).

[31] K. Qu and G. S. Agarwal, Phys. Rev. A **87**, 063813 (2013).

[32] K. Ullah, H. Jing, and F. Saif, Phys. Rev. A **97**, 033812 (2018).

[33] K. Ullah, Eur. Phys. J. D **73**, 267 (2019).

[34] K. A. Yasir and W.-M. Liu, Sci. Rep. **6**, 22651 (2016).

[35] M. J. Akram, F. Ghafoor, and F. Saif, J. Phys. B: At., Mol. Opt. Phys. **48**, 065502 (2015).

[36] S. Zhang, J. Li, R. Yu, W. Wang, and Y. Wu, Sci. Rep. **7**, 1 (2017).

[37] C. Genes, D. Vitali, and P. Tombesi, Phys. Rev. A **77**, 050307(R) (2008).

[38] K. Ullah, Chin. Phys. B **28**, 114209 (2019).

[39] D. Tarhan, S. Huang, and Ö. E. Müstecaplıoğlu, Phys. Rev. A **87**, 013824 (2013).

[40] F. Saif, K. Ullah, and S. Watanabe, in *The IRAGO Conference 2018: A 360-degree Outlook on Critical Scientific and Technological Challenges for a Sustainable Society*, edited by A. Sandhu, J. Sharma, M. Taki, and T. Kishimoto, AIP Conf. Proc. No. 2067 (AIP, New York, 2019), p. 020002.